98-4333

PILOT-INDUCED OSCILLATION PREDICTION WITH THREE LEVELS OF SIMULATION MOTION DISPLACEMENT

Jeffery A. Schroeder*, William W.Y. Chung†, Duc T. Tran*
NASA Ames Research Center
Moffett Field, California

Soren Laforce, Norman J. Bengford
SYRE Logicon
Moffett Field, California

Abstract

Simulator motion platform characteristics were examined to determine if the amount of motion affects pilot-induced oscillation (PIO) prediction. Five test pilots evaluated how susceptible 18 different sets of pitch dynamics were to PIOs with three different levels of simulation motion platform displacement: large, small, and none. The pitch dynamics were those of a previous in-flight experiment, some of which elicited PIOs. These in-flight results served as truth data for the simulation. As such, the in-flight experiment was replicated as much as possible. Objective and subjective data were collected and analyzed. With large motion, PIO and handling qualities ratings matched the flight data more closely than did small motion or no motion. Also, regardless of the aircraft dynamics, large motion increased pilot confidence in assigning handling qualities ratings, reduced safety pilot trips, and lowered touchdown velocities. While both large and small motion provided a pitch rate cue of high fidelity, only large motion presented the pilot with a high fidelity vertical acceleration cue.

Notation

a,b,c	prefilter zeros and poles, rad/sec
a_{model}	model acceleration, ft/sec^2, rad/sec^2
a_{motion}	motion system commanded acceleration, ft/sec^2, rad/sec^2
F(x,y)	variance ratio with x and y degrees of freedom
$F_{lon}, F_{lat}, F_{ped}$	long., lateral stick and pedal force, lbs
$\dot{h}_{td}$	touchdown vertical velocity, ft/sec
K	control system prefilter gain
K_{mot}	motion system filter high-freq gain
K_θ	control system gearing, deg/in
$L_{\delta lat}$	lateral control sensitivity, 1/sec^2/in
$M_{\delta e}$	elevator control sensitivity, 1/sec^2
$N_{\delta lat}$	directional control sensitivity, 1/sec^2/in
n	number of points in each mean
p	probability that effects are random
s	Laplace transform variable, rad/sec
$T_{\theta 1}, T_{\theta 2}$	pitch-to-elevator zero time constants, sec
β	sideslip angle, deg
δ_e	elevator deflection, deg
δ_{ec}	commanded elevator, deg
δ_{ecfilt}	filtered commanded elevator, deg
δ_{estick}	commanded elevator from stick, deg
$\delta_{lon}, \delta_{lat}, \delta_{ped}$	longitudinal, lateral stick and pedal deflection, in
ζ_{dr}	Dutch roll damping ratio
ζ_{mot}	motion filter damping ratio
ζ_p, ζ_{sp}	phugoid and short period damping ratio
ζ_1, ζ_2	control system prefilter damping ratios
ζ_ϕ	complex zero damping ratio in bank-to-aileron transfer function
θ, ϕ	pitch and roll angles, deg
τ_r, τ_s	roll and spiral mode time constants, sec
ω_{dr}	Dutch roll natural frequency, rad/sec
ω_{mot}	motion system filter natural frequency rad/sec
ω_p, ω_{sp}	phugoid and short period natural fr rad/sec

* Aerospace Engineer. Senior Member AIAA.

† Aerospace Engineer. Member AIAA.

ω_1, ω_2 control system prefilter natural frequencies, rad/sec

ω_ϕ complex zero natural freq. in bank-to-aileron transfer function, rad/sec

Introduction

Ground simulation has not been very successful at predicting subsequent in-flight pilot-induced oscillations (PIOs). A recent study recommended that "validating simulation details, protocols, and tasks and collecting and correlating them with flight test results should be given high priority" to improve this simulation weakness.[1]

With two fixed-base simulators of different capabilities, Ref. 2 evaluated the longitudinal PIO tendencies of configurations tested in a PIO flight test study.[3] The simulation results followed the general trend of the in-flight data; however, the worst in-flight configurations were not as severe on either fixed-base simulator.

The purpose of this study was to determine what effect simulator platform motion has on predicting PIOs. Here, three simulator platform motion characteristics were examined: large, small, and no motion. Five pilots flew a landing task with 18 different sets of longitudinal dynamics with each motion configuration. Both pilot-vehicle performance and subjective data were taken and compared with the previous in-flight study.[3]

Apparatus and Tests

Task

The in-flight task was replicated as much as possible.[3] Pilots started at 135 knots and 1.5 nmi from the runway and flew three visual approaches to full touchdown with each configuration. One approach was straight-in, and one each started with a 150-ft left or right lateral offset from the touchdown point. During the approach, pilots were instructed to maintain constant speed and remain on the glidepath (–2.5 degs) and localizer. Deviations were indicated on head-down instruments. At the start of the run, the aircraft was placed 1/2 dot off the desired localizer and glideslope.

For the left and right offsets, pilots held that offset until an automated voice instructed the pilot to "correct." The pilot then maneuvered the aircraft to land on the desired touchdown point. The "correct" command occurred when the runway overrun disappeared from the visual field-of-view, which corresponded to an altitude of 100 ft.

Figure 1 shows the desired touchdown point, which was the near-left corner of the 1000-ft fixed distance marker located to the right of centerline. This desired touchdown point matched the flight-test study. Table 1 gives the performance standards for the task.

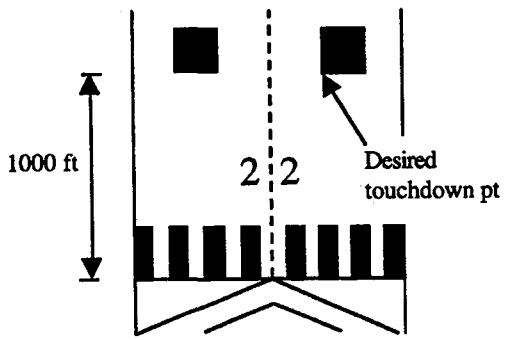

Figure 1 – Landing task

Table 1 – Task performance standards

	Desired	Adequate
PIOs	None	None
Longitudinal touchdown error	+/– 250 ft	+/– 500 ft
Lateral touchdown error	+/– 5 ft	+/– 25 ft
Approach airspeed	+/– 5 kts	–5/+10 kts

Math model

Longitudinal configurations. A linear stability derivative model[4] generated the aerodynamic forces and moments on the aircraft. Bare airframe derivatives were combined from several sources.[3,5,6] Response feedbacks of angle-of-attack and pitch rate to the elevator were used to simulate the different pitch configurations, given below, which mimics the NT-33 variable stability aircraft.[5] Figure 2 shows the dynamic blocks of the pitch axis dynamics.

The simulation centerstick dynamics were measured as:

$$\frac{\delta_{lon}}{F_{lon}}(s) = \frac{0.125(22^2)}{s^2 + 2(0.7)(22)s + 22^2}$$

These dynamics are slower than the 25 rad/sec stick longitudinal natural frequency stated in Refs. 3 and 7 due to force-feel system limitations of this simulator cockpit. The ergonomics of the stick matched Ref. 7.

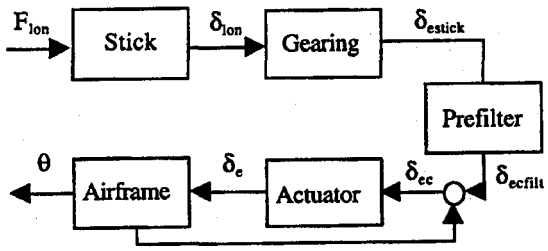

Figure 2 – Longitudinal block diagram

Fourteen prefilters were simulated as in the in-flight experiment. These prefilters consisted of first, second, and fourth-order linear filters. These filters are of the form below, and Table 2 gives their values:

$$\frac{\delta_{e_{c_{filt}}}}{\delta_{e_{stick}}}(s) = \frac{K(s+a)}{s+b}$$

$$\frac{\delta_{e_{c_{filt}}}}{\delta_{e_{stick}}}(s) = \frac{K}{s+c}$$

$$\frac{\delta_{e_{c_{filt}}}}{\delta_{e_{stick}}}(s) = \frac{K}{s^2+2\zeta_1\omega_1 s+\omega_1^2}$$

$$\frac{\delta_{e_{c_{filt}}}}{\delta_{e_{stick}}}(s) = \frac{K}{(s^2+2\zeta_1\omega_1 s+\omega_1^2)(s^2+2\zeta_2\omega_2 s+\omega_2^2)}$$

Table 2 – Control system prefilters

Filter	K	a	b	c	ζ_1	ω_1	ζ_2	ω_2
B	3.0	3.3	10	–	–	–	–	–
D	0.5	20	10	–	–	–	–	–
1	1.0	–	–	–	–	–	–	–
2	10	–	–	10	–	–	–	–
3	4.0	–	–	4	–	–	–	–
5	1.0	–	–	1	–	–	–	–
6	16^2	–	–	–	0.7	16	–	–
7	12^2	–	–	–	0.7	12	–	–
8	9^2	–	–	–	0.7	9	–	–
9	6^2	–	–	–	0.7	6	–	–
10	4^2	–	–	–	0.7	4	–	–
11	16^4	–	–	–	0.93	16	0.38	16
12	2^2	–	–	–	0.7	2	–	–
13	3^2	–	–	–	0.7	3	–	–

Commanded elevator deflection was the sum of the prefilter output and the feedbacks of angle-of-attack and pitch rate. The elevator actuator dynamics were modeled as a second-order filter with the NT-33 rate and position limits.[7] In the linear range, the actuator dynamics are:

$$\frac{\delta_e}{\delta_{e_c}}(s) = \frac{75^2}{s^2+2(0.7)(75)s+75^2}$$

Four sets of aircraft dynamics were evaluated. The differences among the dynamics were effectively in the short-period mode. The pitch-to-elevator transfer function had the following form:

$$\frac{\theta}{\delta_e}(s) = \frac{M_{\delta_e}(s+1/T_{\theta_1})(s+1/T_{\theta_2})}{(s^2+2\zeta_p\omega_p s+\omega_p^2)(s^2+2\zeta_{sp}\omega_{sp}s+\omega_{sp}^2)}$$

Table 3 gives the parameters for the above transfer function. For all configurations, $M_{\delta e}$=–3.3 1/sec^2.

Table 3 – Aircraft dynamics

A/C	$T_{\theta 1}$	$T_{\theta 2}$	ζ_p	ω_p	ζ_{sp}	ω_{sp}
2	12	1.4	0.15	0.17	0.64	2.4
3	12	1.4	0.17	0.16	1.0	4.1
4	12	1.4	0.16	0.16	0.74	3.0
5	12	1.4	0.16	0.15	0.68	1.7

The remaining parameter to be specified is the gearing between the elevator command from the stick and the longitudinal stick position. For the 18 tested configurations, which represent combinations of the aircraft dynamics and prefilters, the gearings are listed in Table 4. As an example, for configuration 2-B, the "2" corresponds to the values in Table 3 and the "B" corresponds to the values in Table 2.

Subsequent to the experiment's start, information from the Ref. 2 authors indicated that the Table 4 gearings may have been 70% higher than in the flight test. To evaluate the effect of different gearings on the results, a mini-experiment was run using the Ref. 2 gearings with configurations 3-1, 3-D, and 3-12. Differences between gearings were less than or equal to one handling qualities and pilot-induced oscillation point.

Each of the 18 configurations was verified by performing frequency sweeps on each and overplotting the result against the analytical pitch-rate-to-stick-deflection transfer functions.

Table 4 - Gearings

Config	K_θ	Config	K_θ
2-B	-2.94	3-8	-7.29
2-1	-2.94	3-12	-7.29
2-5	-4.33	3-13	-7.29
2-7	-2.94	4-1	-3.46
2-8	-2.94	4-2	-3.46
3-D	-8.65	5-1	-1.73
3-1	-7.29	5-9	-1.73
3-3	-7.29	5-10	-1.73
3-6	-7.29	5-11	-1.73

The engine model consisted of a first-order transfer function from throttle input to thrust output. The time constant was nonlinear and depended on RPM.[7]

Lateral. Using a lateral-directional stability derivative model, coefficients were adjusted to achieve the following modal and sensitivity characteristics:

$$\tau_r = 0.3 \text{ sec}$$

$$\tau_s = 75 \text{ sec}$$

$$\omega_{dr} = \omega_\phi = 1.3 \text{ rad/sec}$$

$$\zeta_{dr} = \zeta_\phi = 0.2$$

$$\left|\frac{\phi}{\beta}\right|_{dr} = 1.5$$

$$L_{\delta_{lat}} = 0.7 \text{ rad/sec}^2/\text{in}$$

$$N_{\delta_{ped}} = -0.2 \text{ rad/sec}^2/\text{in}$$

These characteristics were also verified with frequency sweeps.

Atmosphere. Dryden turbulence with rms magnitudes of 3 ft/sec was used. A vertical 1-cosine gust occurred when the aircraft reached an altitude of 100 ft. The gust had a peak of 12 ft/sec and was time scaled based on the 6.7 ft chord of the NT-33.

Safety pilot. Evaluation pilots in the NT-33 flight study were accompanied by a safety pilot, who ended the evaluation and assumed control of the aircraft if a potentially hazardous situation occurred. If a safety pilot assumes control, then questions arise immediately on that configuration's "controllability" from the handling qualities point of view. The presence of a safety pilot can also add a factor of stress, since another set of eyes is watching the evaluation pilot.

In this simulation, an automatic safety pilot was implemented that assumed control of the simulated model when the nosewheel's vertical speed exceeded –8 ft/sec below a center-of-mass height of 12 feet. This criterion was developed empirically and was well received by the pilots. Upon activation, the pilot's controls went dead, a voice said "my airplane," and the math model initiated a go-around.

Simulator

Motion system. The NASA Ames Vertical Motion Simulator (VMS) was used.[8] It is the world's largest-displacement flight simulator, with capabilities shown in Figure 3. The cockpit was oriented for large longitudinal travel. The dynamics of the motion system were measured during the experiment using frequency response testing techniques.[9] These dynamics were fit with an equivalent time delay in each axis. Software feedforward filters were used to tune the delays to achieve a close match among axes. The equivalent time delays for the surge, sway, pitch, roll, and yaw axes were all 80 msecs, and the heave axis had 110 msec of delay. By comparison, delays in the NT-33 model following control system have been suggested as being in the 45-60 msec range.

VMS Nominal operational motion limits

Axis	Displ	Velocity	Accel
Vertical	± 30	16	24
Longitudinal	± 20	8	16
Lateral	± 4	4	10
Roll	± 18	40	115
Pitch	± 18	40	115
Yaw	± 24	46	115

All numbers, units ft, deg, sec

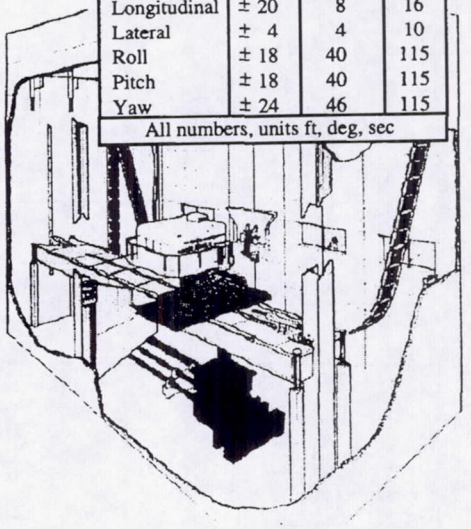

Figure 3 – NASA Ames Vertical Motion Simulator

Visual system. The visual scene was rendered with an Evans & Sutherland ESIG-3000 image generator. Three monitors comprised the field of view, as shown

in Fig. 4. The visual system had a measured time delay of 80 msec from the pilot's stick position to the visual scene. Figure 5 shows the visual scene with the aircraft near the runway. The nose of the simulated aircraft is at the bottom of the field-of-view. Window mullions were added (oval in Figure 5) to replicate the cockpit.[7]

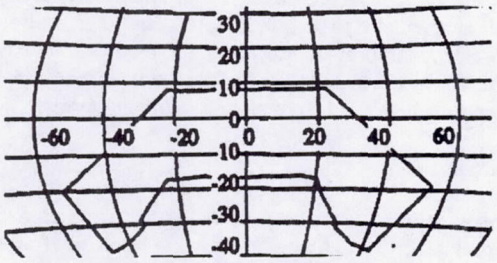

Figure 4 – Cockpit field-of-view

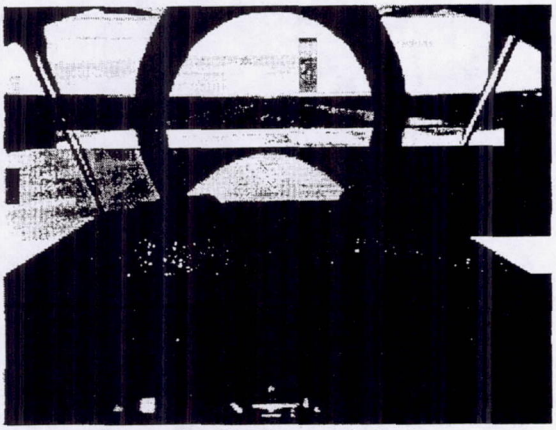
Figure 5 – Simulator cockpit photo

Cockpit. The lateral stick and pedal dynamics were measured as:

$$\frac{\delta_{lat}}{F_{lat}}(s) = \frac{0.25(16^2)}{s^2 + 2(0.7)(16)s + 16^2}$$

$$\frac{\delta_{ped}}{F_{ped}}(s) = \frac{0.0167(25^2)}{s^2 + 2(0.7)(25)s + 25^2}$$

A head-up display was video mixed with the visual scene. The display included a pitch ladder, altitude above sea level, airspeed, rate-of-climb, heading, range, and a flightpath marker. The flightpath marker represented center-of-mass flightpath and used raw data only.

Motion configurations

Three motion configurations were examined: large, small, and no motion. The VMS motion platform software was modified to implement each.

Large motion. The classical washout motion control laws of the VMS were used for this configuration. Second-order high-pass (washout) filters exist between the math model accelerations and the commanded motion system accelerations. These filters have the form:

$$\frac{a_{motion}}{a_{model}}(s) = \frac{K_{mot}s^2}{s^2 + 2\zeta_{mot}\omega_{mot}s + \omega_{mot}^2}$$

In each of the six motion degrees-of-freedom, both K_{mot} and ω_{mot} were adjusted to keep the motion system within its displacement limits using motion system fidelity criteria suggested initially by Sinacori[10] and revised and validated subsequently.[11] Table 5 shows the values used. The damping ratio, ζ_{mot}, was 0.7. In addition to these cues, roll/sway coordination and residual tilt crossfeeds were present in the motion logic.[12]

Table 5 - Large motion system parameters

Axis	K_{mot}	ω_{mot}
Pitch	1.00	0.20
Roll	0.40	0.50
Yaw	0.65	0.20
Longitudinal	0.65	0.40
Lateral	0.50	0.50
Vertical	0.80	0.30

Small motion. A coordinated-adaptive algorithm, used on many of today's hexapods, was employed in the small motion configuration.[13,14] This algorithm assumed a mathematical model of a hexapod platform with 60-in stroke actuators. Thus, the stroke limiting that occurs when commanding several axes was present. Euler angles and translational positions of the platform were back solved on line from the resulting (and potentially limited) actuator positions.[15] The Euler angles and positions were then used to drive the VMS platform.

Second-order high-pass filters were used in the translational axes, while the rotational axes used a first-order high-pass filter (unlike the Large motion configuration). The second-order filters had a damping ratio of 0.7, except for the surge axis, which was 0.8. For comparison, Table 6 gives the gains and natural

frequencies (or pole locations) for the small motion filters. The gains listed are the maximum values, as the coordinated-adaptive algorithm reduces these values when the actuators near their travel limits. These gains were adjusted to use as much of the 60-in actuator stroke as possible.

Table 6 – Small motion system parameters

Axis	K_{mot}	ω_{mot} (or pole)
Pitch	0.50	0.30 (pole)
Roll	0.25	0.81 (pole)
Yaw	0.70	0.30 (pole)
Longitudinal	0.11	0.67
Lateral	0.45	0.90
Vertical	0.13	0.90

No motion. The motion system was turned off in this configuration.

Comparison with fidelity criteria. Figure 6 plots each axis of the large and small motion configurations against the validated criteria of Ref. 11. These points are determined by finding the magnitude and phase of the respective motion filter evaluated at 1 rad/sec.

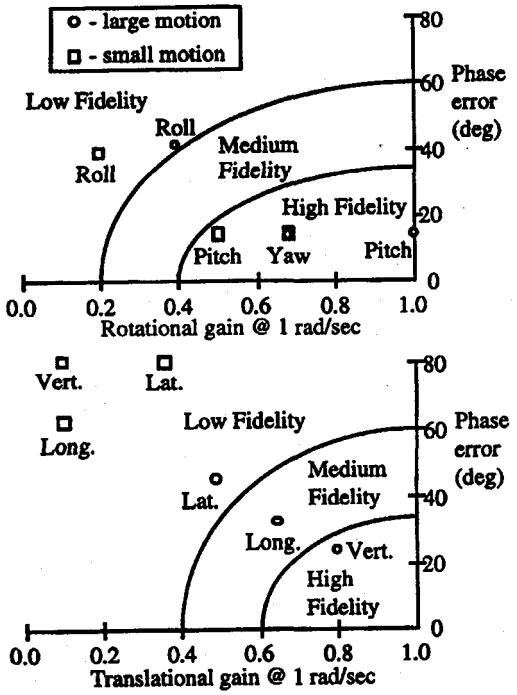

Figure 6 – Motion fidelity prediction

In the rotational axes, high motion fidelity is predicted for both pitch and yaw motion with the large and small motion configuration. Roll motion is low fidelity in both motion configurations, since the roll axis was attenuated to minimize the false lateral specific force cueing during coordinated rolling maneuvers.

In the translational axes, all of the small motion cues are predicted to be low fidelity. For large motion, the fidelity improves, especially for the vertical axis, which provides a key cue for this task. This figure shows the benefit of large motion in fidelity terms.

Pilots

Five experience test pilots, hereafter referred to as A-E, participated. Pilot A was an FAA test pilot, pilots B-D were NASA Ames test pilots, and pilot E was a Boeing test pilot.

Experimental procedure

Summarizing the experimental variables, they were:

1. motion configuration (3),
2. aircraft configuration (18)

Thus, each pilot evaluated 54 configurations. Pilots A, B, and E evaluated each configuration at least twice. Pilots C and D evaluated each configuration only once.

The pilots each read the same experimental briefing. They had no knowledge of the configurations, which were randomized. After flying the task, the pilots were told of their performance. Then, they assigned a handling qualities rating using the Cooper-Harper scale,[16] a Pilot Confidence Factor,[16] and a Pilot Induced Oscillation Rating (PIOR).[6]

Results and Discussion

Objective data

Example PIO. Figure 7 illustrates a classic divergent PIO that occurred with Pilot B, configuration 3-12, and large motion. The pilot was nearly on the longitudinal stick stops. The pilot gave this configuration a Cooper-Harper rating of 8, and a PIO rating of 5. PIOs of this severity and for this extended period of time did not occur for either the small or no motion configurations.

The average frequency of the PIO in Figure 7 is 3.0 rad/sec (the average in-flight PIO frequency of this

configuration was 2.2 rad/sec). Also shown on the pitch rate and normal acceleration traces are the motions that both the large and small motion configurations would produce for this visual motion.

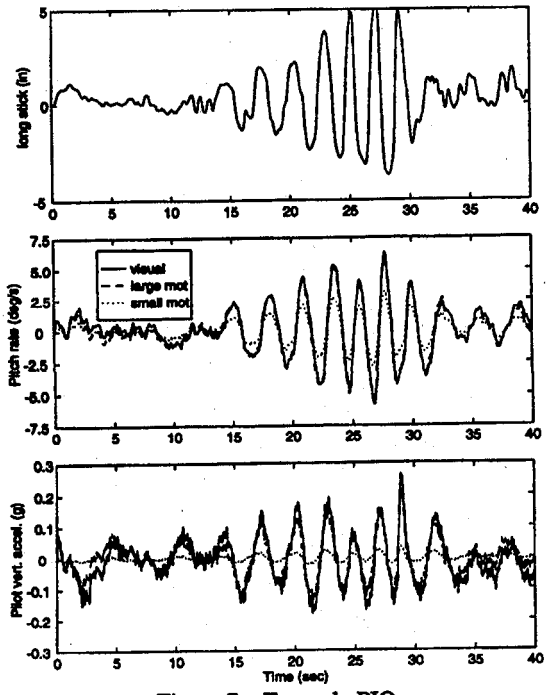

Figure 7 – Example PIO

At the PIO frequency, the large motion configuration provides 100% of the pitch rate cue, and it leads the visual scene by only 5 degs of phase angle. So, the dashed line overlays the solid line. These values may be determined by inserting 3 rad/sec into the motion system filter discussed earlier with the pitch axis parameters (Table 5). The small motion configuration, at best, provides 50% of the visual pitch rate and leads the visual by 6 degs. By motion cueing fidelity standards, both the large and small motion cues are high fidelity.[10,11]

For the normal acceleration, the large motion configuration provides 80% of the visual cue and leads the visual by 3 degs (this value includes the motion filter and the additional 30 msec of delay that the vertical platform lags the visual). But the small motion configuration provides only 13% of the visual cue and leads the visual by 20 degs. By motion cueing fidelity standards, the large motion cue would be high fidelity, and the small motion cue would be low fidelity. It is for this important acceleration cue that large motion provides a simulation benefit, and it is likely the reason for the superior performance of the large motion configuration as discussed later.

Landing performance. Longitudinal touchdown position was analyzed using a two-way repeated measures analysis of variance (ANOVA).[17] While statistically significant differences occurred across the aircraft configurations ($F(17,68)=3.73$, $p<0.001$), differences among the motion configurations were not found ($p>0.2$).

Lateral touchdown position was analyzed, and no significant differences were noted among the aircraft ($p>0.4$) or motion configurations ($p>0.4$). Approach airspeed errors were almost always within the desired performance standard.

During the evaluations, it was noticed that pilots had difficulty in judging sink rate during the flare-to-touchdown as less platform motion was presented. Indications of this fact were either harder landings or the safety pilot assuming control for the small and no motion configurations.

Figure 8 shows the means and standard deviations of vertical touchdown velocities for each motion configuration. Each mean is an average of 90 points (18 configurations x 5 pilots). The ANOVA on these data indicated that the motion configuration affected touchdown velocity independent of the vehicle configuration ($F(2,8)=36.8$, $p<0.001$).[17] Aircraft configuration also affected touchdown velocity independent of motion configuration ($F(17,68)=2.93$, $p<0.001$). No interaction between the motion and vehicle configurations was present ($p>0.3$). Thus, touchdown velocity could be modeled as independent functions of the motion and aircraft configurations:

$$\dot{h}_{td} = f(\text{motion}) + g(\text{aircraft})$$

As more motion was available, pilots were able to lower the touchdown velocity. A previous limited experiment with large motion also indicated this effect when the longitudinal handling qualities were poor;[18] however, the results here indicate that large motion allows lower touchdown velocities regardless of the configuration.

As Table 1 notes, sink rate at touchdown was not a performance parameter in this experiment, which was also the case in the Ref. 3 flight experiment. However, the Ref. 2 simulation experiment added a touchdown performance criterion of $\leq$ 4 ft/sec for desired performance and $\leq$ 8 ft/sec for adequate performance. Had that been the case here, it is expected that even further differences among the motion configurations would

have occurred. This is because when more platform motion was added, it compensated for sink rate perception deficiencies in the visual scene.

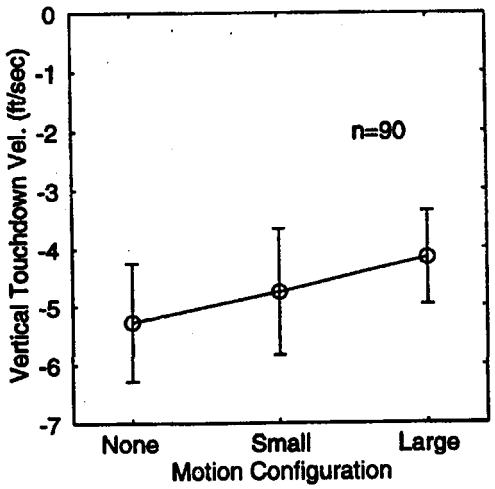

Figure 8 – Touchdown velocities

Safety pilot trips. Figure 9 shows the number of times the automated safety pilot assumed control versus the motion configuration. Over 1400 landings were performed, so the safety pilot assumed control in approximately 10% of the landings. It took control slightly fewer times with small motion than with no motion; however, large motion resulted in significantly fewer safety pilot trips. Many of the safety pilot trips occurred from the inability to judge sink rate.

While it was stated earlier that causing the safety pilot to assume control should raise questions about the configuration's controllability, this seldom occurred. Pilots often felt they were still in control. The issue was that the small or no motion configurations did not assist pilots in their estimation of vertical velocity as did the large motion cues.

Stick activity. Longitudinal stick rms positions were analyzed. Statistical differences occurred across aircraft configurations ($F(17,68)=7.81$, $p<0.001$), with configurations 5-10 and 3-12 having the most activity (0.96 and 0.93 in, respectively). Configurations 2-B and 3-D had the least activity (0.49 and 0.51 in, respectively). No significant differences occurred across the motion configurations ($p>0.1$).

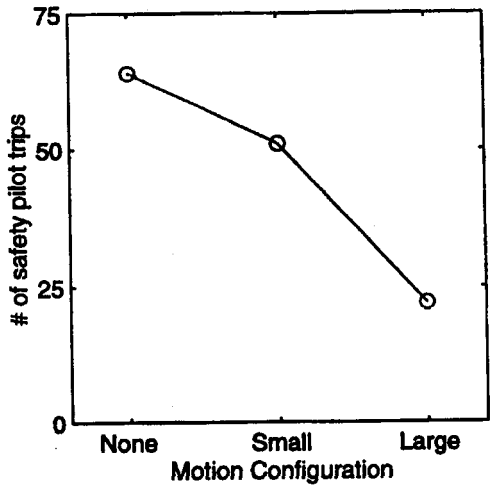

Figure 9 – Safety pilot trips

Handling Qualities Ratings

Large Motion. Figure 10 is a plot of the in-flight HQRs[3] versus the simulation HQRs for the large motion condition. If simulation matched flight, then all points would lie on the diagonal line. A 1-unit HQR band is plotted about this line, which is often taken as the range of an acceptable match. Eight of the 18 configurations lie within this 1-unit band. Very similar trends to that of the Ref. 2 fixed-based simulation are noted. That is, the best configurations in flight were slightly worse in simulation, and the worst configurations in flight were better in simulation.

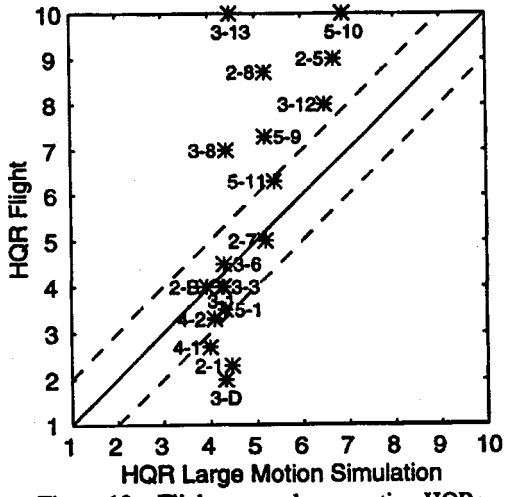

Figure 10 – Flight versus large motion HQRs

Small Motion. Figure 11 shows the in-flight versus simulation HQRs for small motion. Six of the 18 configurations lie within the 1-unit band, which is a degradation from the large motion condition. Again, the same trend on the best and worst configurations existed as for large motion.

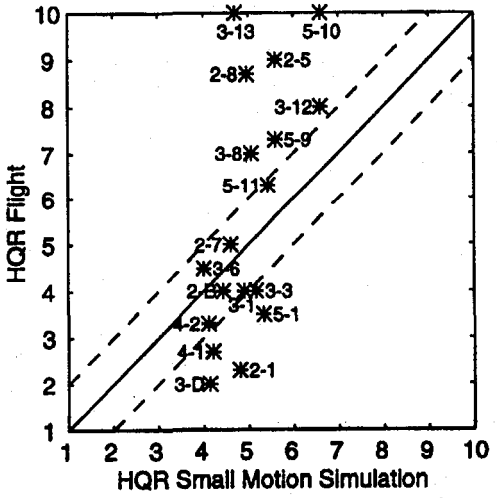

Figure 11 – Flight versus small motion HQRs

No Motion. Figure 12 shows the in-flight versus simulation HQRs for no motion. Five of the 18 configurations were within the 1-unit band, which is a degradation from large motion and small motion. Again, the same trend on the best and worst configurations existed as for large and small motion.

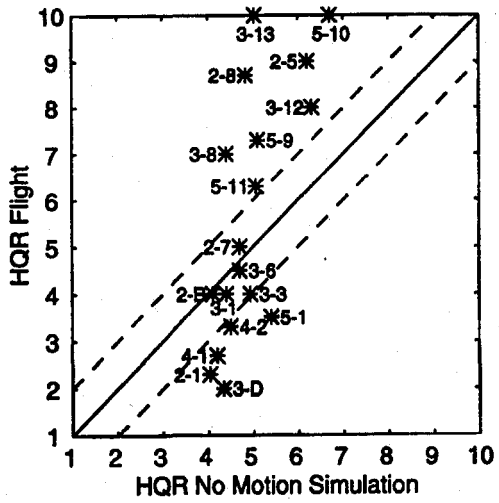

Figure 12 – Flight versus no motion HQRs

Pilot Confidence Factors. Confidence factors of A, B, and C refer to a pilot's opinion that he can assign a handling qualities rating with a high, moderate, or minimum degree of confidence, respectively.[16] Losses of confidence arise when simulation cues are incomplete or inadequate. Figure 13 shows that as more motion is provided, the pilot's confidence in assigning ratings improves. On average, both the no motion and small motion configurations caused the pilot to have less than a moderate degree of confidence in his rating. With large motion, that confidence improved to more than moderate. This difference was statistically significant across the motion configurations ($F(2,8)=5.82$, $p=0.028$). Differences in this measure were not significant across the aircraft configurations ($p>0.1$).

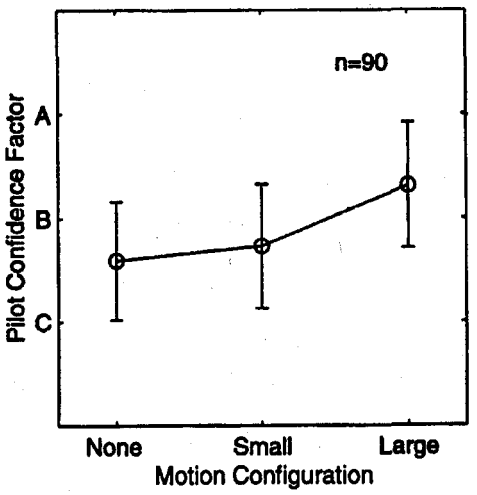

Figure 13 – Pilot confidence factors

PIO Ratings

Large motion. Figure 14 compares pilot-induced oscillation ratings (PIORs) between flight and the large motion simulation. Sixteen of the 18 configurations lie inside the +/– 1 PIOR boundary. Except for four configurations, the in-flight PIORs were, on average, higher than the simulation PIORs.

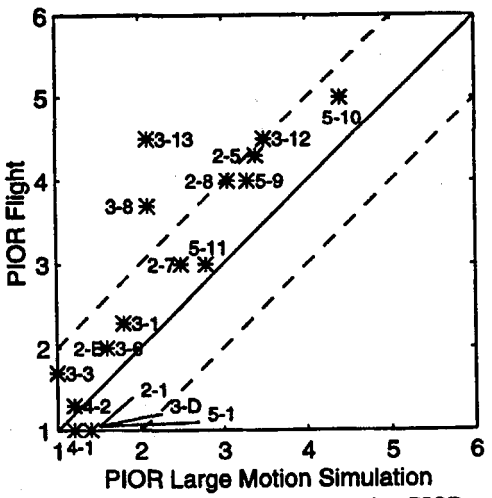

Figure 14 – Flight versus large motion PIORs

Small motion. PIORs for the small motion configuration are shown in Figure 15. Here, 12 configurations were inside the +/– 1 PIOR band, which was the worst performance of the motion configurations. Again, except for four configurations, the in-flight PIORs were worse than the simulator PIORs.

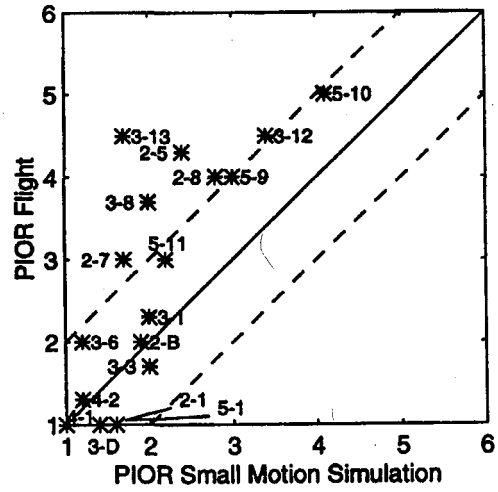

Figure 15 – Flight versus small motion PIORs

No motion. The PIORs for no motion are given in Figure 16. No motion performed slightly better than small motion, but worse than large motion. Fourteen configurations were inside the +/– 1 PIOR band. Still, except for four configurations, the in-flight PIORs were higher than the no motion PIORs.

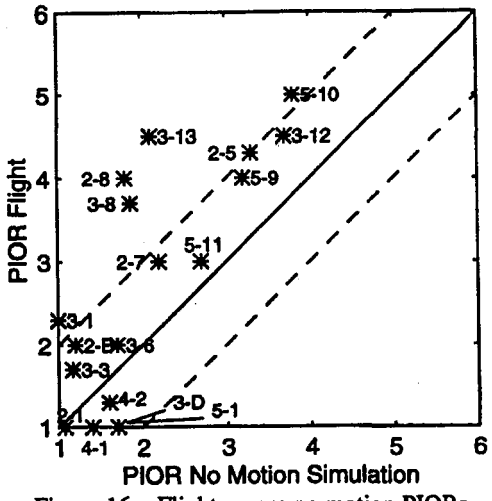

Figure 16 – Flight versus no motion PIORs

Conclusions

A piloted experiment examined the effect of three levels of platform motion displacement on the ability to predict pilot-induced oscillations. Objective and subjective measures were examined for large, small, and no platform motion. The small motion condition represented the displacement of a conventional hexapod platform.

Overall, large motion matched flight more closely than either small or no motion. Specifically, large motion better matched the in-flight pilot-induced oscillation ratings and the handling qualities ratings than did small or no motion. In addition, with large motion, pilots assigned higher confidence factor ratings, achieved lower touchdown velocities, and caused fewer safety pilot trips as compared to the other motion configurations. Finally, only with large motion did markedly divergent pilot-induced oscillations occur.

An example illustrated that high fidelity pitch rate cues were provided by both the large and small motion configurations. However, only large motion allowed high fidelity vertical acceleration cues to be presented. Pilots react strongly to vertical acceleration, and this likely contributed to the large motion configuration providing the best results.

References

1. National Research Council Committee on the Effects of Aircraft-Pilot Coupling on Flight

Safety, *Aviation Safety and Pilot Control – Understanding and Preventing Unfavorable Pilot-Vehicle Interactions*, National Academy Press, Washington, D.C., 1997.

2. Kish, B.A., Leggett, D.B., Nguyen, B.T., Cord, T.J., Slutz, G.J., "Concepts for Detecting Pilot-Induced Oscillation Using Manned Simulation," AIAA Paper 96-3431, San Diego, CA, 1996.

3. Bjorkman, E.A., "Flight Test Evaluation of Techniques to Predict Pilot Induced Oscillations," Masters Thesis, AFIT/GAE/AA/86J-1, Air Force Institute of Technology, Dec., 1986.

4. McRuer, D., Ashkenas, I., and Graham, D., *Aircraft Dynamics and Automatic Control*, Princeton University Press, Princeton, NJ, 1973, pp. 203-295.

5. Hall, G.W. and Huber, R.W., "System Description and Performance Data for the USAF/CAL Variable Stability T-33 Airplane," AFFDL-TR-70-71, Wright-Patterson Air Force Base, OH, Aug. 1970.

6. Smith, R.E., "Effects of Control System Dynamics on Fighter Approach and Landing Longitudinal Flying Qualities – Volume I," AFFDL-TR-78-122, Wright-Patterson Air Force Base, OH, Mar., 1978.

7. Buethe, S.A., Govindaraj, K.S., and Knotts, L.H., "Description of NT-33A Configurations for Use in Programming NASA Vertical Motion Simulator (VMS)," Calspan Report No. 7205-5, Calspan Corporation, Buffalo, NY, Mar., 1984.

8. Danek, G., "Vertical Motion Simulator Familiarization Guide," NASA TM 103923, May, 1993.

9. Tischler, M.B. and Cauffman, M.G., "Frequency-Response Method of Rotorcraft System Identification: Flight Applications to BO-105 Coupled Rotor/Fuselage Dynamics," *Journal of the American Helicopter Society*, Vol. 37, No. 3, pp. 3-17, July, 1992.

10. Sinacori, J.B., "The Determination of Some Requirements for a Helicopter Flight Research Simulation Facility," NASA CR-152066, Sept. 1977.

11. Schroeder, J.A., "Helicopter Flight Simulation Motion Requirements," Ph.D. Dissertation, Stanford University, May, 1998.

12. Rolfe, J.M. and Staples, K.J., *Flight Simulation*, Cambridge University Press, Cambridge, 1986.

13. Parrish, R.V., Dieudonne, J.E., Bowles, R.L., and Martin, Jr., D.J., "Coordinated Adaptive Washout for Motion Simulators," *Journal of Aircraft*, Vol. 12, No. 1, Jan., 1975, pp. 44-50.

14. Martin, Jr., D.J., "A Digital Program for Motion Washout on Langley's Six-Degree-of-Freedom Motion Simulator," NASA CR 145219, July, 1977.

15. Dieudonne, J.E., Parrish, R.V., and Bardusch, R.E., "An Actuator Extension Transformation for a Motion Simulator and an Inverse Transformation Applying Newton-Raphson's Method," NASA TN D-7067, 1972.

16. Cooper, G.E. and Harper, Jr., R.P., "The Use of Pilot Rating in the Evaluation of Aircraft Handling Qualities," NASA TN D-5153, Apr., 1969.

17. Myers, J.L., *Fundamentals of Experimental Design*, Allyn and Bacon, Inc., Boston, 1972, pp. 167-190.

18. Bray, R.S., "A Study of Vertical Motion Requirements for Landing Simulation," *Human Factors*, Vol. 15, No. 6, Dec., 1973, pp. 561-568.